Propulsion of catalytic Janus spheres in viscosified Newtonian solutions

Purba Chatterjee, Edmund M. Tang, Pankaj Karande, and Patrick T. Underhill

Phys. Rev. Fluids **3**, 014101 — Published 8 January 2018

DOI: 10.1103/PhysRevFluids.3.014101

Propulsion of catalytic Janus-spheres in viscosified Newtonian solutions

Purba Chatterjee,[1] Edmund M. Tang,[1] Pankaj Karande,[1] and Patrick T. Underhill[1, *]
[1] *Department of Chemical and Biological Engineering, Rensselaer Polytechnic Institute,*
110 8th St, Troy, New York 12180, USA
(Dated: December 19, 2017)

The propulsion of active colloids made from silica microspheres half-coated with platinum is experimentally probed in solutions of hydrogen peroxide as a function of solution viscosity. The velocity is shown to decay approximately inversely with viscosity. Further, the type of viscosifier used affects the interaction between fuel molecules and motor which affects propulsion. The quantification of how a viscosifier alters both viscosity and interactions is interpreted using existing diffusion-reaction models of self-diffusiophoresis.

I. INTRODUCTION

The influence of the swimming medium on propulsion at low Reynolds (Re) number has been observed for a large number of swimming microorganisms [1, 2]. Numerous mechanisms and mathematical models have been proposed to explain the motion of biological swimmers [1, 3, 4]. Beyond the biological realm, studies on low Re number motion of artificial swimmers have also been carried out, as reviewed by Lauga and Powers [1]. They categorized such engineered bio-inspired systems based on whether they deform in a non reciprocal manner or use chemical reactions to power locomotion such as catalytic Janus particles. The use of Janus particles to make active motors has received much attention in the last decade. These self-propelled micro/nano-swimmers have applications in designing sensors which respond to external stimuli [5–7] and in carrying and dropping cargo [7, 8] that can be useful in drug delivery and nanomedicine [9–11].

The methods to control the random motion of catalytic motors have been reviewed by Wang *et al.* [12]. Phoretic swimmers move under the influence of external fields [13–15]. Concentration gradients of solutes/fuels across a particle's interfacial region also result in diffusiophoresis [16], and self-diffusiophoresis is one of the widely accepted mechanisms of such propulsion. Ionic effects and motion by self-electrophoresis have also been examined, which sometimes dominate the propulsion mechanism [17, 18]. Hong *et al.* [19] report chemotaxis of Platinum-Gold rods, where they "actively diffused" along a gradient towards higher hydrogen peroxide due to catalysis. Others have looked into the direction of propulsion of these Janus motors [20, 21]. Recent studies have looked into additional aspects of the nature of particle propulsion. Howse *et al.* [22] show propulsion of half platinum-coated microspheres in an aqueous solution of H_2O_2 as a function of fuel concentration. Ebbens *et al.* [23] demonstrate how, over the experimentally accessible range, motor size can affect propulsion at a given fuel concentration.

Many applications of such motors involve moving objects through complex environments that are mixtures of components, such as body fluids for drug delivery applications. The flow properties of these mixtures could be Newtonian or non-Newtonian. In other applications, additives may be introduced as a way of controlling the motion of motors. The first step in understanding how the fluid mixtures alter their motion is to examine propulsion in fluids where additives change the shear viscosity while the fluid remains Newtonian. Most of the reported active motors propel in aqueous solutions [22–24], although some studies have been performed in non-Newtonian fluids [25]. In this article, we show how solution viscosity affects Janus motor propulsion keeping all other factors (motor size, fuel concentration, temperature, etc.) constant. This is part of the overall goal of understanding how solution properties impact propulsion independent of a particular application.

II. METHODS AND MODELS

We use carboxylated ($-COOH$) silica microspheres (0.96 μm average diameter) purchased from BangsLabs (SC04N/11632). A particle suspension in deionized water is deposited on cleaned microscope glass slides using "convective assembly" of colloidal particles [26] to obtain submonolayer coverage. A thin layer of platinum (Pt) ($\approx 5\ nm$) is deposited onto the particles using e-beam evaporation. The metal half is used to catalyze the decomposition of hydrogen peroxide (fuel) into water and oxygen. These half coated particles are detached from the glass slides by

---

* Corresponding author: underhill@rpi.edu

sonication in deionized water and re-dispersed in 1mM MES (2-(N-morpholino)ethanesulfonic acid) buffer (pH = 4.4 - 6.7) after obtaining suitable concentrations by centrifugation. A dye attachment reaction is performed whereby the surface carboxyl groups on the non-metal half of these particles are covalently conjugated with a fluorescent dye, Alexa Fluor 633 hydrazide (Life Technologies A30634), having an excitation wavelength of 633 nm. This enables imaging and tracking of the Janus particles by fluorescence microscopy. The fluorescent Janus particles are dispersed as a stock solution in 1mM phosphate buffer (pH = 7.4) at a concentration of about 2 mg/ml. Hydrogen peroxide solutions are prepared from suitable dilutions of 30% (w/w) stock solutions (Sigma-Aldrich, 216763). We have used two different viscosifiers: sucrose (> 99% Sigma, S2395) and glycerol (99.7%, Soapgoods, 56-81-5). The solution viscosities are adjusted (verfied using a rheometer) by using suitable volumes of viscosifiers from their respective stock solutions.

A cuvette (3.5 ml nominal volume and 1 cm optical path length - Fisher Scientific, 14-385-902C) is rinsed and sonicated with deionized water and 100 wt% ethanol before usage and sealed with a PTFE stopper. The total working volume is 2 ml which has a Janus particle concentration of about 2.5×10^{-4} mg/ml in 1mM phosphate buffer. All experiments have been performed at $29°C$. Particle tracking is done at 40X magnification using a Zeiss Axio Observer Z1 inverted epifluorescence microscope, mounted on an isolation table and a Xcite 120Q series mercury lamp for illumination. The videos are recorded using an Andor Zyla 3-tap CMOS camera at 40 frames per second (fps) with the field of view of 1280×1080 pixels where the image resolution is 0.31 microns/pixel. For each viscosity at a given H_2O_2 concentration, approximately 30 separate particles are tracked and analyzed using the Interactive Data Language (IDL) software developed by Crocker and Grier [27] yielding the particle trajectories in 2D which are used to calculate their Mean Square Displacements (MSDs). These silica-Pt Janus particles have a higher density than the suspending solution and eventually settle near the bottom of the cuvette resulting in a more effective 2D tracking and analysis. Each particle is analyzed independently to obtain a velocity, diffusivity, etc. All experimental data presented here are the mean of the values of each particle with error bars corresponding to plus and minus the standard error (computed as the standard deviation divided by the square root of the number of particles).

Howse *et al.* [22] have described how the propulsion alters the random walk of a particle, which is quantified in terms of how its MSD (ΔL^2) depends on the lag time (Δt). For a particle undergoing passive Brownian motion with diffusivity D_{Br} in addition to propulsion with speed V in which the orientation of the propulsion decorrelates with rotational time τ_r, the two dimensional MSD is

$$\Delta L^2 = 4D_{Br}\Delta t + \frac{V^2\tau_r^2}{2}\left(\frac{2\Delta t}{\tau_r} + e^{\frac{-2\Delta t}{\tau_r}} - 1\right). \tag{1}$$

The Brownian diffusivity is given by the Stokes-Einstein-Sutherland equation: $D_{Br} = kT/6\pi\eta a$, where k is the Boltzmann constant, T is the absolute temperature, η is the solution viscosity and a is the particle radius. The rotational time τ_r, is the reciprocal of the rotational diffusion coefficient D_r and is given by Stokes-Einstein-Debye equation for a sphere of radius a, $\tau_r = 8\pi\eta a^3/kT$. Note that this is the two dimensional MSD of a particle whose orientations are free to move in all three directions and V^2 is the mean squared projected velocity. If the orientations are restricted, it can lead to the same functional form but a different value for the rotational decorrelation time.

The limiting behaviors of this MSD at short and long time are used to fit the experimental data. For $\Delta t \ll \tau_r$ the first terms in the Taylor series are

$$\Delta L^2 = 4D_{Br}\Delta t + V^2\Delta t^2, \tag{2}$$

which is the combination of passive diffusion and ballistic propulsive motion. For $\Delta t \gg \tau_r$ the direction of propulsion changes randomly, which leads to diffusive motion. This gives a MSD that behaves approximately as

$$\Delta L^2 = (4D_{Br} + V^2\tau_r)\Delta t - \frac{V^2\tau_r^2}{2}. \tag{3}$$

The effective long-time diffusivity is

$$D_L = D_{Br} + \frac{V^2\tau_r}{4}. \tag{4}$$

A quadratic fit at short times is used to obtain the short time diffusivity and the velocity. A linear fit at long times is used to obtain the long time diffusivity. The regions of lag time to fit must be chosen carefully. At short times, a narrow fit region is more prone to statistical errors while a wide fit region may extend past the quadratic region. Our short time fits are over the region of lag time from zero to one-quarter of the theoretical value of τ_r. The long time fit must be in the region that the MSD becomes linear while statistical errors are small. Our long time fits are over the region of lag time from the theoretical value of τ_r to 2.5 times the theoretical value of τ_r.

A number of theoretical models have been proposed to guide the design of a Janus motor [17, 18, 28, 29]. Recent studies have used the addition of salts to examine the contributions of self-electrophoresis versus self-diffusiophoresis [17, 18]. At the ionic strengths of the buffer used here, the ionic contributions are reduced. Furthermore, because many surface groups have been reacted with a dye for visualization the surface charge of our particles is not high, which also reduces the contributions from ionic effects. Therefore, we will use self-diffusiophoresis to interpret the experimental results. It has been shown by Brady [30] that in some limits a colloidal approach and a continuum approach to self-diffusiophoresis using reaction-diffusion models yield the same result for the propulsive velocity. The important features of the theory are the dependence on surface reaction rate and fuel concentration that are typically common among propulsion mechanisms.

The reaction on half of the surface creates a concentration gradient of reactants and products around the particle that exerts a force on the particle. This force is balanced by the viscous drag of the particle moving through the fluid. The Peclet number ($Pe = V(a + a_s)/D_{H_2O_2}$) quantifies how strongly the particle speed alters the concentration distribution, where a_s is an effective radius of a hydrogen peroxide molecule and $D_{H_2O_2}$ is its diffusivity. In all cases examined here, Pe is very small which simplifies the theory.

The concentration profile around a Janus motor is determined by the Damköhler number (Da) that compares the reaction at the surface to diffusion to the surface. For a reaction that is effectively first order with rate constant κ, $Da = \kappa(a + a_s)/D_{H_2O_2}$. The theoretical prediction for the speed of the motor for small and large Da are [30]

$$V \approx \begin{cases} \frac{CkTb^2}{4\pi\eta a} Da, & \text{for } Da \to 0 \\ \frac{CkTb^2}{4\pi\eta a}, & \text{for } Da \to \infty \end{cases} \tag{5}$$

where C is the concentration of the reactant far from the particle and b is a parameter with units of length that quantifies the strength and range of interactions between the solutes and particle surface. The viscosity appears explicitly in the formula for the velocity, but also appears indirectly because the diffusivity of hydrogen peroxide (which is inside Da) also depends on viscosity.

There is some uncertainty regarding the expected range of Da for our experiments. The scaling of speed with particle radius observed in literature [23] is consistent with theories if Da is above one. However, two studies that directly measured kinetics produce rates that give Da closer to 0.01 [17, 18]. We are not aware of a theory that predicts the particle radius scaling observed when Da is small. Alternatively, it may be that different ways of producing the particles can cause variations in reaction rates. It is also important to understand the roles of mixing and interactions when interpreting kinetic measurements. Ref. [17] measured the decrease in weight from evolution of oxygen gas from a cuvette containing a suspension of the Janus particles. The distribution of motors within the cuvette including aggregates could lead to an underestimation of the reaction rate. Ref. [18] measured the reaction rate over a $1cm^2$ square of deposited Platinum. Because of the size of the square, diffusion limitations may play a role in the measurement. If the kinetics are inferred from a diffusion-limited situation, then used to calculate Da with a smaller size, the value of Da will be smaller than the correct value. To overcome diffusion limitations over the $1cm^2$ square, external flow could be applied. The only flow present in the kinetic experiments of ref. [18] is the flow naturally generated due to the reaction.

Because of the uncertainty in the Da, we will interpret our data in two ways. The first is to assume very low Da even at the highest viscosity used. The second is to use a theory that includes the whole range of possible Da and use the experimental data to infer the Da, including how it changes as the viscosity changes. This approximate velocity theory is

$$V \approx \frac{CkTb^2}{4\pi\eta a} \frac{Da}{1 + Da}. \tag{6}$$

This formula is not exact but combines the small and large Da expressions and gives a transition between the two limits similar to the calculations in [29].

III. RESULTS AND DISCUSSION

If the parameters κ and b were constants, then the velocity would be independent of viscosity at low Da and would be inversely proportional to viscosity at high Da. Therefore, it is helpful to present the measured velocity both directly and as velocity times viscosity. Figure 1 shows the velocity in solutions with either 3M or 4M H_2O_2 and varying viscosity using either sucrose or glycerol added to water. The overall trend is that the velocity drops during the addition of sucrose or glycerol. The details of the dependence and the error bars can be seen more easily on the plot of velocity times viscosity.

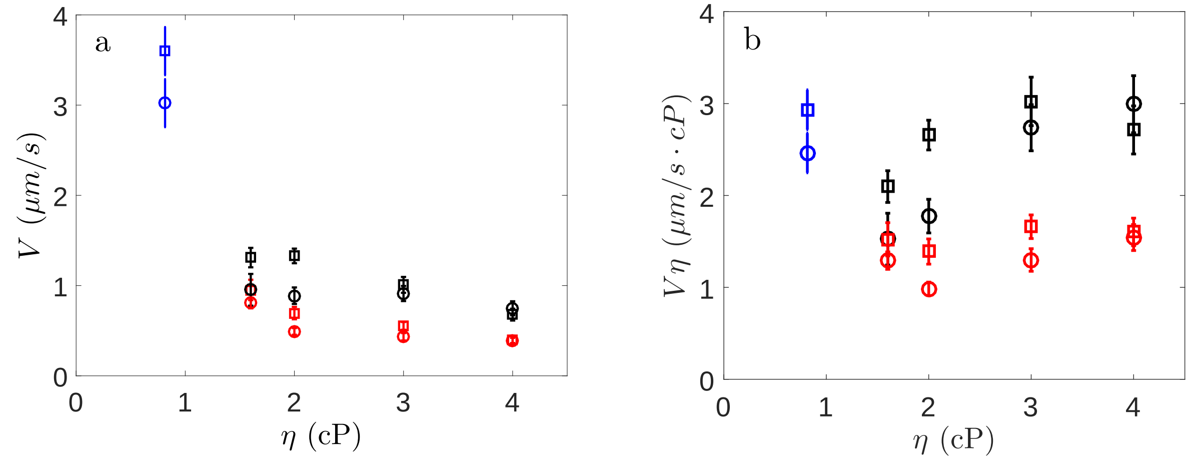

FIG. 1. (color online) Velocity V of the silica-Pt Janus spheres in solutions of varying viscosity obtained from quadratic fits using Eq. (2). Data are shown as velocity directly (a) and velocity times viscosity (b). The concentration of hydrogen peroxide is 3M (circles) and 4M (squares). *Blue:* Data points in aqueous solutions; *Black:* Data points with sucrose as viscosifier; *Red:* Data points with glycerol as viscosifier.

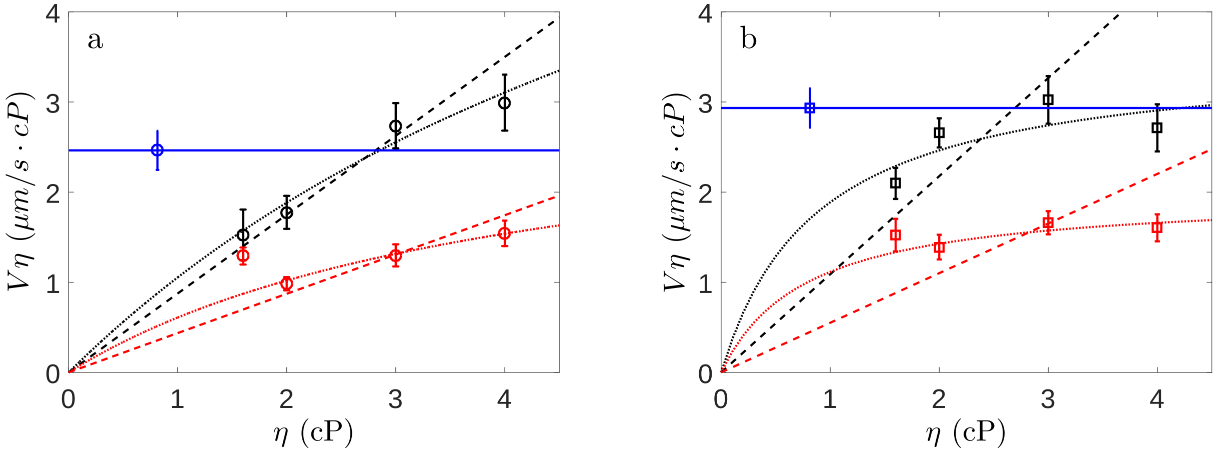

FIG. 2. (color online) Data of velocity times viscosity shown separately for (a) 3M H_2O_2 and (b) 4M H_2O_2. The horizontal blue solid lines are simply provided as guides to the eye. The dashed lines are the lines of best fit using the low Da equation in equation 5 and the dotted lines are the lines of best fit using equation 6. *Blue:* Data points in aqueous solutions; *Black:* Data points with sucrose as viscosifier; *Red:* Data points with glycerol as viscosifier.

A quantitative analysis of the dependence is best illustrated separately for the 3M and 4M H_2O_2 cases, shown in Figure 2 (a) and (b) respectively. Note that the data in Figures 1(b) and 2 are the same. They are provided separately to help with comparing the data sets and comparing with the fits. The dashed lines are best fits to the data in sucrose or glycerol (excluding the data in water) assuming very low Da and constant κ and b. This gives a reasonable fit to the data at 3M H_2O_2 but not for 4M H_2O_2. One interpretation of the data is that the Da is very small and that any deviation from the straight lines is due to the reaction rate κ and/or interaction parameter b that depend on the amount of sucrose or glycerol present in solution. This is possible, although it would be surprising that these dependencies would combine in some situations to give a velocity times viscosity nearly independent of viscosity (the large Da behavior).

Therefore, we also analyze the data using equation 6 that contains both low and high Da behaviors. Again we assume that κ and b are constants while the sucrose or glycerol are added, but they can be different from the values in water and they can be different in 3M and 4M H_2O_2. As the viscosity increases, the value of Da changes due to changes in $D_{H_2O_2}$ such that $Da \propto \eta$. By fitting the data, we can obtain both the proportionality factor and a value of b. These fits are shown in dotted curves.

For 3M H_2O_2 the fits give $b = 0.84$Å for sucrose and $b = 0.50$Å for glycerol, while the Damköhler numbers are $Da = 0.13(\eta/1cP)$ for sucrose and $Da = 0.24(\eta/1cP)$ for glycerol. The resulting values of Da are less than one,

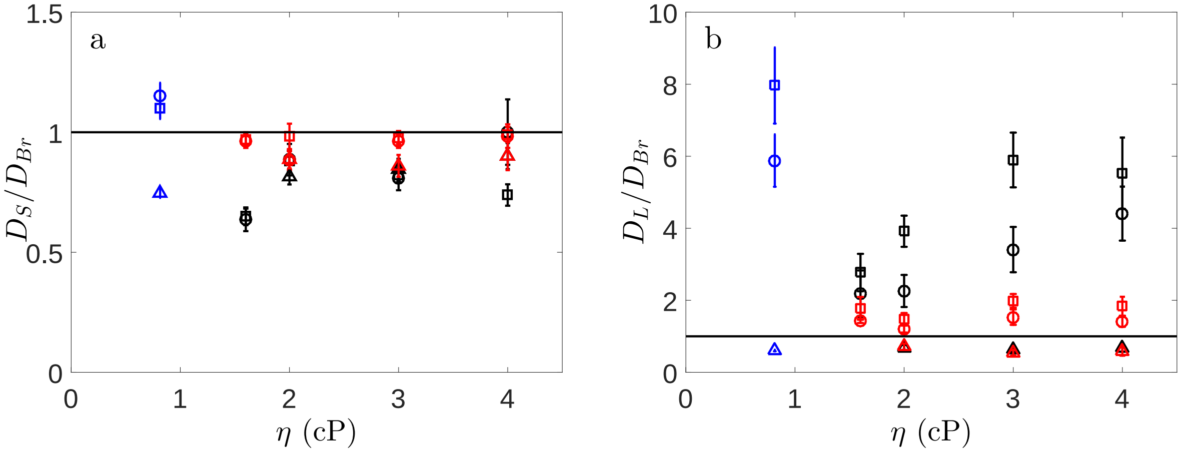

FIG. 3. (color online) (a) D_S/D_{Br} vs viscosity where D_S has been determined from quadratic fits to MSD for $\Delta t \ll \tau_r$ (Eq. (2)). The solid line is shown at a value of 1. (b) D_L/D_{Br} vs viscosity where D_L has been determined from linear fits to MSD for $\Delta t \gg \tau_r$ (Eq. (3)). The solid line is shown at a value of 1. *Blue:* Data points in aqueous solutions; *Black:* Data points with sucrose as viscosifier; *Red:* Data points with glycerol as viscosifier. The hydrogen peroxide concentrations are 0M (triangles), 3M (circles), and 4M (squares).

but become close enough to one at the high viscosity that the fits are not straight lines. For 4M H_2O_2 the fits give $b = 0.46$Å for sucrose and $b = 0.34$Å for glycerol, while the Damköhler numbers are $Da = 1.1(\eta/1cP)$ for sucrose and $Da = 1.3(\eta/1cP)$ for glycerol. The resulting values of Da are greater than one, but are close enough to one at the low viscosity that the fits are not horizontal lines. The overall interpretation from this type of analysis is that the presence of sucrose and glycerol alter the interactions of peroxide with the surface and the reaction rate, which leads to a drop in V and $V\eta$. As more viscosifier is added, the value of Da increases which can transition the response from a low Da behavior to a high Da behavior. This progression is qualitatively the same between sucrose and glycerol. It is currently unclear what about the size and chemistry of sucrose and glycerol that leads to the quantitative differences.

The short and long time diffusivities are also functions of the viscosity of the solution. The short time diffusivity is obtained along with the velocity from a fit similar to Eq. (2) but allowing for a nonzero intercept (I_S) which is small and representative of the static and dynamic errors that arise during particle tracking [31]. The long time diffusivity is obtained from a fit similar to Eq. (3). The nonzero intercept of the long time fit (I_L) is primarily due to the propulsion of the particles.

Figure 3 (a) shows the short time diffusivities scaled by the theoretical Brownian diffusivity, since it is expected from Eq. (2) that the short time diffusivity will equal the Brownian diffusivity. The triangles show the result of "control" experiments in which there is no peroxide and hence no propulsion. They show that the short time diffusivity is consistently approximately 0.8 times the theoretical Brownian diffusivity. This reduction is likely due to the presence of the particles near the glass wall which should reduce their diffusivity [32]. The short time diffusivity in solutions with hydrogen peroxide (and so with propulsion) are typically slightly larger than the control values but are still near the theoretical Brownian value. This increase is likely due to two effects: the reaction could slightly push the particles away from the wall reducing the "wall effect", and the quadratic behavior of the MSD from propulsion can make it difficult to accurately obtain the linear coefficient during the fitting process.

Figure 3 (b) shows the long time diffusivities. They are also scaled by the theoretical Brownian diffusivity to show how the propulsion enhances the motion. The triangles again show the control experiments without peroxide, and show as expected that the long time diffusivity is close to the short time diffusivity; there is no propulsion to enhance the diffusion. The experiments with peroxide show an enhancement in aqueous solution as well as when sucrose or glycerol is added. The theoretical expectation for D_L/D_{Br} comes from combining equation (4) with the theories for V and τ_r. If the Da were small, we would predict a quadratic increase. If the Da were large, we would predict a constant value.

If we examine the viscosified systems separately from the data in water, the trends are consistent with that found with the velocity. That is, the data with 3M H_2O_2 appear close to the low Da theory (nearly quadratic) at smaller viscosity with a change at higher viscosity. However, the data with 4M H_2O_2 more quickly level off at higher viscosity consistent with a larger Da.

To understand the role of the rotational diffusion time, we can deduce an effective τ_r from the MSD data. One approach is to use Eq. (4) written as $D_L = D_S + V^2\tau_r/4$ to calculate an effective τ_r from the values of D_L, D_S, and V obtained from the fits. The other approach to estimate an effective τ_r is using the intercepts from the short

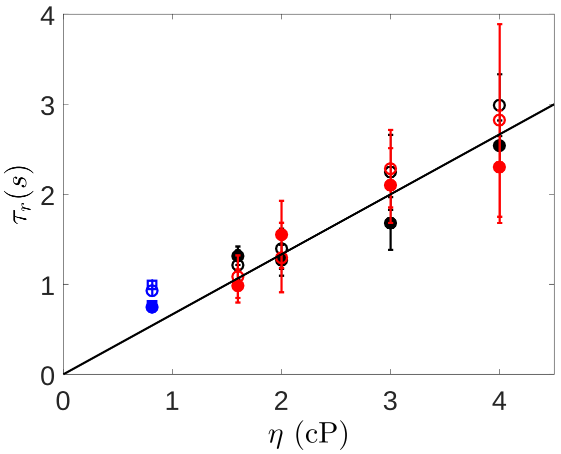

FIG. 4. (color online) Rotational time τ_r of the silica-Pt Janus spheres in 3M H_2O_2 solutions of varying viscosity. Two different methods have been used: Using the short and long time diffusivities (open symbols); Using the intercepts from quadratic and linear fits (filled symbols). The solid line is the theoretical prediction of τ_r as a function of viscosity using Stokes-Einstein-Debye equation. *Blue:* Data points in aqueous solutions; *Black:* Data points with sucrose as viscosifier; *Red:* Data points with glycerol as viscosifier.

and long time fits. Equation (3) showed that the long time intercept was affected by propulsion. This approach uses the intercepts to estimate $\tau_r = 2(I_S - I_L)/V^2$. Figure 4 shows the rotational times inferred from the MSD data. The data extracted from the two methods are similar and show that the effective τ_r increases with viscosity. In the viscosified solutions, the τ_r matches with the theoretical expectation within statistical errors. Notably, the values in aqueous solution are higher that the theoretical value, an observation also noted by Ke *et al.* [20] for their silica-Pt Janus particles at high H_2O_2 concentrations. Slower rotations lead to a larger long time diffusivity than would be predicted based on the theoretical τ_r. This slower rotation may be due to an active mechanism similar to that described previously [33, 34] in which motors primarily propel in directions nearly parallel to a planar wall. This restriction effectively eliminates a degree of freedom to decorrelate orientations which increases the decorrelation time. It also leads to particles that continually have a half-moon appearance. In our results, a half-moon shape does occur, but not over the entire movies. The return of τ_r to the theoretical values in viscosified fluids suggests that such an active mechanism is suppressed by the high viscosity. This is possibly because the active mechanisms typically scale with the speed, which is smaller in the viscosified solutions (see Fig. 1(a)).

IV. CONCLUSION

We have shown how adding viscosifiers can affect propulsion of Janus motors. Even if the fluid remains Newtonian, the amount of propulsion not only depends on fluid viscosity but also the chemical nature of the viscosifying agent. The viscosifier can affect the surface reaction rate, which will affect the Damköhler number. The viscosifier can also alter how the reactants and products interact with the particle, thereby altering the parameter b if interpreted using the theory of self-diffusiophoresis. For very small Da, changes in the reaction rate and effective interactions combine together so they cannot be distinguished from measurements of the velocity alone. An alternative interpretation of our results is that the Da is close to order one and varies with viscosity. This approach allows us to estimate the actual values of Da and b. Future kinetic measurements in the presence of sucrose and glycerol will examine the mechanistic details of how different molecules can alter the reactions, provided the kinetic measurements are done in a way that they minimize interactions between particles and diffusion limitations. Future studies will also examine Janus motors in non-Newtonian environments. In these more complex environments, the effective resistance to translational motion (which affects V) and effective resistance to rotational motion (which affects τ_r) could be different. Similarly, the effective viscosity in the diffusivity of small solutes like the reactant will likely be different from the effective viscosity for the translational motion of the motor.

ACKNOWLEDGMENTS

The authors thank Prof. Sufei Shi for the ebeam evaporation of Platinum on silica microspheres for the synthesis of Janus particles. We gratefully acknowledge the National Science Foundation (NSF) Grant No. CBET-1544617 for their support.

---

[1] Eric Lauga and Thomas R Powers, "The hydrodynamics of swimming microorganisms," Reports on Progress in Physics **72**, 096601 (2009).
[2] Alison E Patteson, Arvind Gopinath, and Paulo E Arratia, "Active colloids in complex fluids," Current Opinion in Colloid & Interface Science **21**, 86–96 (2016).
[3] Yukio Magariyama and Seishi Kudo, "A mathematical explanation of an increase in bacterial swimming speed with viscosity in linear-polymer solutions," Biophysical journal **83**, 733–739 (2002).
[4] Howard A Stone and Aravinthan DT Samuel, "Propulsion of microorganisms by surface distortions," Physical review letters **77**, 4102 (1996).
[5] Timothy R. Kline, Walter F. Paxton, Thomas E. Mallouk, and Ayusman Sen, "Catalytic nanomotors: Remote-controlled autonomous movement of striped metallic nanorods," Angewandte Chemie International Edition **44**, 744–746 (2005).
[6] Prajnaparamita Dhar, Yanyan Cao, Timothy Kline, Priya Pal, Cheryl Swayne, Thomas M. Fischer, Brian Miller, Thomas E. Mallouk, Ayusman Sen, and Tom H. Johansen, "Autonomously moving local nanoprobes in heterogeneous magnetic fields," The Journal of Physical Chemistry C **111**, 3607–3613 (2007).
[7] Rawiwan Laocharoensuk, Jared Burdick, and Joseph Wang, "Carbon-nanotube-induced acceleration of catalytic nanomotors," ACS Nano **2**, 1069–1075 (2008), pMID: 19206505.
[8] Shakuntala Sundararajan, Paul E. Lammert, Andrew W. Zudans, Vincent H. Crespi, and Ayusman Sen, "Catalytic motors for transport of colloidal cargo," Nano Letters **8**, 1271–1276 (2008), pMID: 18416540.
[9] Debabrata Patra, Samudra Sengupta, Wentao Duan, Hua Zhang, Ryan Pavlick, and Ayusman Sen, "Intelligent, self-powered, drug delivery systems," Nanoscale **5**, 1273–1283 (2013).
[10] Daniel Kagan, Rawiwan Laocharoensuk, Maria Zimmerman, Corbin Clawson, Shankar Balasubramanian, Dae Kang, Daniel Bishop, Sirilak Sattayasamitsathit, Liangfang Zhang, and Joseph Wang, "Rapid delivery of drug carriers propelled and navigated by catalytic nanoshuttles," Small **6**, 2741–2747 (2010).
[11] Wei Gao and Joseph Wang, "Synthetic micro/nanomotors in drug delivery," Nanoscale **6**, 10486–10494 (2014).
[12] Joseph Wang and Kalayil Manian Manesh, "Motion control at the nanoscale," Small **6**, 338–345 (2010).
[13] Peer Fischer and Ambarish Ghosh, "Magnetically actuated propulsion at low reynolds numbers: towards nanoscale control," Nanoscale **3**, 557–563 (2011).
[14] Nicolas Mano and Adam Heller, "Bioelectrochemical propulsion," Journal of the American Chemical Society **127**, 11574–11575 (2005).
[15] Yang Wang, Rose M Hernandez, David J Bartlett, Julia M Bingham, Timothy R Kline, Ayusman Sen, and Thomas E Mallouk, "Bipolar electrochemical mechanism for the propulsion of catalytic nanomotors in hydrogen peroxide solutions," Langmuir **22**, 10451–10456 (2006).
[16] John L Anderson, "Colloid transport by interfacial forces," Annual review of fluid mechanics **21**, 61–99 (1989).
[17] Aidan Brown and Wilson Poon, "Ionic effects in self-propelled pt-coated janus swimmers," Soft matter **10**, 4016–4027 (2014).
[18] S Ebbens, DA Gregory, G Dunderdale, JR Howse, Y Ibrahim, TB Liverpool, and R Golestanian, "Electrokinetic effects in catalytic platinum-insulator janus swimmers," EPL (Europhysics Letters) **106**, 58003 (2014).
[19] Yiying Hong, Nicole M. K. Blackman, Nathaniel D. Kopp, Ayusman Sen, and Darrell Velegol, "Chemotaxis of nonbiological colloidal rods," Phys. Rev. Lett. **99**, 178103 (2007).
[20] Hua Ke, Shengrong Ye, R Lloyd Carroll, and Kenneth Showalter, "Motion analysis of self-propelled pt- silica particles in hydrogen peroxide solutions," The Journal of Physical Chemistry A **114**, 5462–5467 (2010).
[21] Stephen J Ebbens and Jonathan R Howse, "Direct observation of the direction of motion for spherical catalytic swimmers," Langmuir **27**, 12293–12296 (2011).
[22] Jonathan R Howse, Richard AL Jones, Anthony J Ryan, Tim Gough, Reza Vafabakhsh, and Ramin Golestanian, "Self-motile colloidal particles: from directed propulsion to random walk," Physical review letters **99**, 048102 (2007).
[23] Stephen Ebbens, Mei-Hsien Tu, Jonathan R Howse, and Ramin Golestanian, "Size dependence of the propulsion velocity for catalytic janus-sphere swimmers," Physical Review E **85**, 020401 (2012).
[24] Stephen J. Ebbens and Jonathan R. Howse, "In pursuit of propulsion at the nanoscale," Soft Matter **6**, 726–738 (2010).
[25] Juan Ruben Gomez-Solano, Alex Blokhuis, and Clemens Bechinger, "Dynamics of self-propelled janus particles in viscoelastic fluids," Physical review letters **116**, 138301 (2016).
[26] Brian G Prevo and Orlin D Velev, "Controlled, rapid deposition of structured coatings from micro-and nanoparticle suspensions," Langmuir **20**, 2099–2107 (2004).
[27] John C Crocker and David G Grier, "Methods of digital video microscopy for colloidal studies," Journal of colloid and interface science **179**, 298–310 (1996).

[28] R Golestanian, T B Liverpool, and A Ajdari, "Designing phoretic micro- and nano-swimmers," New Journal of Physics **9**, 126 (2007).

[29] Ubaldo M Córdova-Figueroa and John F Brady, "Osmotic propulsion: the osmotic motor," Physical review letters **100**, 158303 (2008).

[30] John F Brady, "Particle motion driven by solute gradients with application to autonomous motion: continuum and colloidal perspectives," Journal of Fluid Mechanics **667**, 216–259 (2011).

[31] Thierry Savin and Patrick S. Doyle, "Static and dynamic errors in particle tracking microrheology," Biophysical Journal **88**, 623 – 638 (2005).

[32] John Happel and Howard Brenner, *Low Reynolds number hydrodynamics: with special applications to particulate media*, Vol. 1 (Springer Science & Business Media, 2012).

[33] Sambeeta Das, Astha Garg, Andrew I Campbell, Jonathan Howse, Ayusman Sen, Darrell Velegol, Ramin Golestanian, and Stephen J Ebbens, "Boundaries can steer active janus spheres," Nature communications **6**, 8999 (2015).

[34] Juliane Simmchen, Jaideep Katuri, William E Uspal, Mihail N Popescu, Mykola Tasinkevych, and Samuel Sánchez, "Topographical pathways guide chemical microswimmers," Nature communications **7**, 10598 (2016).